

Designing Amorphous Networks with Adjustable Poisson Ratio from a Simple Triangular Lattice


Zhipeng Jin^{1,2}, Chenchao Fang^{1,2,4}, Xiangying Shen^{3,*} and Lei Xu^{1,2,†}

¹*Department of Physics, The Chinese University of Hong Kong, Hong Kong, People's Republic of China*

²*Shenzhen Research Institute, The Chinese University of Hong Kong, Shenzhen 518057, People's Republic of China*

³*Department of Materials Science and Engineering, Southern University of Science and Technology (SUSTech), Shenzhen 518055, People's Republic of China*

⁴*Shenzhen JL Computational Science and Applied Research Institute, Shenzhen 518131, People's Republic of China*

 (Received 4 May 2022; revised 17 September 2022; accepted 29 September 2022; published 17 November 2022)

Materials with a negative and tunable Poisson ratio have great potential applications in fracture resistance and energy absorption. However, one material usually exhibits one specific Poisson ratio and a systematic tuning is highly desired. In this study, we design disordered networks with a wide tunable range of the Poisson ratio based on triangular analysis. By distorting the equilateral triangle lattice, the Poisson ratio can be systematically decreased due to the large area change in highly nonequilateral triangles. Analysis further shows that in a nonequilateral triangle, bonds with different lengths play distinct roles: the removal of short bonds can decrease the Poisson ratio, while the removal of long bonds does the opposite. Thus a negative Poisson ratio can be achieved by removing a small amount of short bonds. Moreover, such networks can serve as unit cells to build larger systems with a similar performance. Such auxetic networks are further experimentally realized in both spring and three-dimensionally printed systems, demonstrating the general validity of our analysis and its possible applications in building practical systems.

DOI: [10.1103/PhysRevApplied.18.054052](https://doi.org/10.1103/PhysRevApplied.18.054052)

I. INTRODUCTION

Different materials exhibit very different elastic properties, the bulk modulus (B) and shear modulus (G) of which may vary over many orders of magnitude [1]. However, their Poisson ratio, proposed by Poisson [2] and defined as the ratio between the transverse strain (ε_t) perpendicular to and the longitudinal strain (ε_l) along the loading direction, $\nu = -\varepsilon_t/\varepsilon_l$, differs within a narrow range for isotropic materials [1,3,4]. For isotropic materials, the Poisson ratio is determined by the bulk and shear moduli, B and G [5,6]: $\nu_{\text{iso}} = (dB/G - 2)/[d(d - 1)B/G + 2]$ where d is the system dimensionality. Apparently, it has a narrow range of $-1 \leq \nu \leq 1/(d - 1)$, since B and G are generally positive. There are also a great number of studies on the Poisson ratio of amorphous or disordered materials [7–10]. Natural materials typically exhibit a positive Poisson ratio, while negative Poisson ratios (i.e., auxetic [11] materials) are rare. However, due to the excellent mechanical

properties of auxetic materials in fracture resistance and energy absorption, it is important to design and realize such materials.

Dating back to 1987, the first reported auxetic material had a reentrant foam structure [12]. Since then, a variety of artificial auxetic materials have been proposed, the negative Poisson ratios of which are induced by their unique structures. They are classified into several categories according to different mechanisms [3,4]: reentrant structure [13–15], rotating polygonal structure [16–18], chiral structure [19–21], crumpled sheets [22–24], and perforated sheets [25,26]. At the same time, more and more natural auxetic materials and structures are also being reported [27–32]. These artificial and natural auxetic materials show great potential applications in the field of smart sensors [33], indentation and fatigue resistance [34], filters [35], and soft electronics [36].

Most of the artificial auxetic materials belong to cellular structures. They can be considered as a lattice network consisting of many nodes connected by bonds. Such a lattice network typically exhibits a specific Poisson ratio. Therefore, if we want to obtain a series of Poisson ratios, we need to design a series of different structures. As a result, such auxetic materials cannot adjust themselves

*Correspondence should be addressed to shenxy@sustech.edu.cn

†Correspondence should be addressed to xuleixu@cuhk.edu.hk

flexibly according to changes in external conditions and behave as an intelligent system. However, recent studies [37–41] show that the Poisson ratio can be systematically varied in amorphous networks by removing a series of bonds. Compared to auxetic materials based on periodic cellular structures, the amorphous networks are more powerful in tunability by using one framework structure to achieve a series of auxetic materials with continuous Poisson ratios. In this study, we illustrate a theoretical mechanism of tuning the Poisson ratio in a simple triangle and design adjustable auxetic materials with triangles arranged in a disordered manner. Our system can either decrease or increase the Poisson ratio continuously by, respectively, removing short and long bonds in triangles. Such systems are further experimentally realized in both spring and three-dimensionally (3D) printed networks, demonstrating the general validity of our

analysis, and its possible applications in building practical systems.

II. TUNING THE POISSON RATIO INSIDE A TRIANGLE

We first explore the mechanical properties of a regular lattice of identical triangles with N nodes and N_B bonds, as shown in Fig. 1(a). For simplicity, all the bonds are to be considered as ideal springs with the spring constants k_1 , k_2 , and k_3 . Obviously, this simple network has a unit triangle ABC , with its interior angles (α, β) and orientation angle (θ) shown in Fig. 1(b) inset. Such a triangular lattice has the coordination number $z \equiv 2N_B/N = 6$ and exhibits a completely affine mechanical response, i.e., under a specific strain imposed on the boundary, all internal node positions deform linearly with respect to their

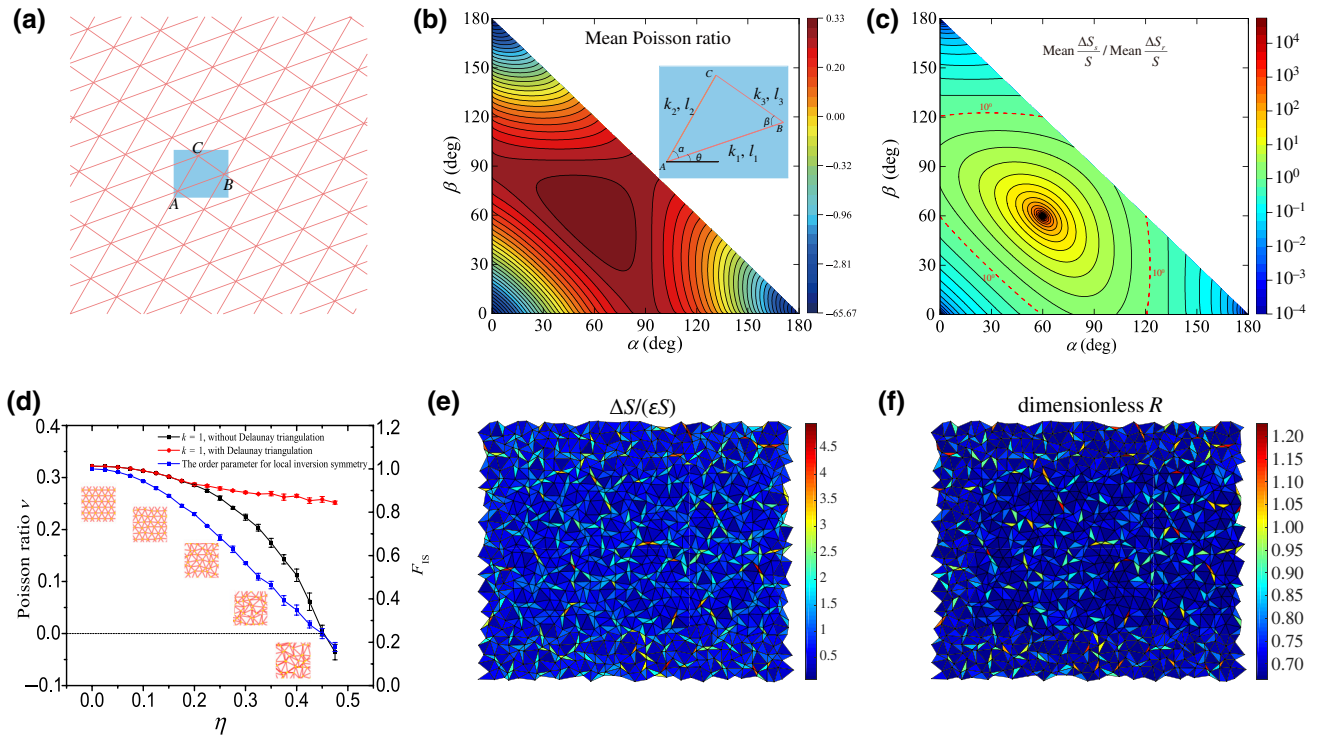


FIG. 1. (a) A regular lattice of triangles with a unit cell ABC . (b) While the inset shows the unit cell ABC of the lattice with interior angles α and β and orientation angle θ , the main panel shows the mean Poisson ratio of the lattice, averaged over all orientations θ , at different interior angles α and β . Negative ν appears at three corners. Note that very negative values below -1 can be reached because the regular lattice is anisotropic, while amorphous networks are isotropic, with ν limited above -1 . (c) The area change from bond stretching versus the area change from bond relative rotation: stretching dominates near the center of the equilateral region, while relative rotation dominates near the three corners. (d) Distortion of the equilateral triangle lattice reduces ν to negative values (black symbols). However, reconnecting the network with Delaunay triangulation, which avoids large deviations from an equilateral triangle, makes ν quite stable (red symbols). The order parameter of inversion symmetry F_{IS} (blue symbols) referred to in Ref. [43] shows a similar trend with the black symbols. (e) The color map of the mean area change in each triangle, renormalized by its original area. (f) The color map of the dimensionless circumcircle radius: $R = \sqrt{3} / [4 \cos(\alpha/2) \cos(\beta/2) \cos(\gamma/2)]$, where α , β , and γ are the three interior angles of the triangle [44]. The two color maps in (e) and (f) are in excellent agreement, indicating a large area change in highly nonequilateral triangles.

distance to the boundary. Therefore, when the network is under external strain ε_y and ε_x along the x and y directions, respectively, we can express its total elastic energy E as $E = E(\alpha, \beta, \theta, \varepsilon_y, \varepsilon_x, l_1, k_1, k_2, k_3)$, where the interior angles α and β , bond lengths l_1 , l_2 , and l_3 , and orientation angle θ are geometric parameters, while k_1 , k_2 , and k_3 are the spring constants of the bonds. Because the relationship between two perpendicular strains ε_x and ε_y can be deduced by minimizing E , we can obtain the Poisson ratio from the definition $\nu = -\varepsilon_l/\varepsilon_l$. For example, we can apply a strain ε_y to the network top and bottom boundaries and let the system relax to an equilibrium state under this strain (i.e., minimizing E); we can then obtain the transverse strain ε_x by measuring the new positions of the left and right boundaries: $\varepsilon_x \stackrel{\partial E/\partial \varepsilon_x=0}{=} \varepsilon_x(\varepsilon_y)$. Then, the Poisson ratio can be calculated: $\nu_{yx} = \lim_{\varepsilon_y \rightarrow 0} -\varepsilon_x(\varepsilon_y)/\varepsilon_y$. The calculated Poisson ratio depends on the triangle geometry and orientation and the spring constants: $\nu = \nu(\alpha, \beta, \theta, k_1, k_2, k_3)$. The detailed derivation can be found in Sec. I of the Supplemental Material [42].

To further simplify this system, we let $k_1 = k_2 = k_3 = k = 1$. In the Supplemental Material [42], we show that the variation in the spring constant does not affect our general results. The Poisson ratio can then be analytically derived as

$$\nu_{yx} = \left\{ 1 - \frac{2[3 + f(\alpha, \beta) + 2g_1(\alpha, \beta, \theta)]}{f(\alpha, \beta) - g_2(\alpha, \beta, \theta)} \right\}^{-1},$$

$$\nu_{xy} = \nu_{yx}(\alpha, \beta, \theta + \pi/2), \quad (1)$$

in which $f(\alpha, \beta) = \cos(2\alpha) + \cos(2\beta) + \cos[2(\alpha + \beta)]$, $g_1(\alpha, \beta, \theta) = \cos[2(\beta - \theta)] + \cos(2\theta) + \cos[2(\alpha + \theta)]$, and $g_2(\alpha, \beta, \theta) = \cos[2(\beta - 2\theta)] + \cos[2(\alpha + 2\theta)] + \cos[2(\alpha - \beta + 2\theta)]$ (see the Supplemental Material [42]). Note that this regular network is anisotropic and that the Poisson ratio depends on the orientation angle θ , except for one particular case, $\alpha = \beta = \gamma = 60^\circ$: the Poisson ratio of such a network is $1/3$ and is independent of θ . Because our goal is to build an isotropic amorphous system composed of triangles in various orientations, we average over all possible orientation angles θ in Eq. (1): $\bar{\nu}(\alpha, \beta) = \int_{-\pi/2}^{\pi/2} \nu_{yx} d\theta/\pi = \int_{-\pi/2}^{\pi/2} \nu_{xy} d\theta/\pi$, which only depends on interior angles α and β . We plot the numerical values of $\bar{\nu}(\alpha, \beta)$ in Fig. 1(b): an island exists in the contour map, centered at the special case $\alpha = \beta = \gamma = 60^\circ$ with the maximum Poisson ratio of $1/3$. More interestingly, the further the triangle deviates from the equilateral triangle, the smaller the Poisson ratio will be, and it reaches negative values at three corners. The three corners correspond to triangles with a large angle close to π (i.e., obtuse triangles).

Next, we illustrate why a negative ν appears in those obtuse triangles. In general, the Poisson ratio correlates to

the area change of the system under an external stretching strain ε : $\nu = 1 - \Delta S/(\varepsilon S)$, where S is the original area and ΔS is the area change under stretching. Apparently, when the system area increases sufficiently under fixed stretching, the perpendicular direction has to expand and thus the Poisson ratio is negative. For a regular lattice of triangles, the total area change is the sum of the area change in each triangle, $\Delta S = \sum_i \Delta S_i$. For an individual triangle ABC , its area is $S = (1/2)ab \sin C$ and the area change is $\Delta S_i = (1/2)\Delta ab \sin C + (1/2)a\Delta b \sin C + (1/2)ab \cos C \Delta C$. The first two terms are caused by the bond-length change (stretching or compression), while the third term is caused by the angle change or relative rotation between the bonds. Thus $\Delta S_i = \Delta S_s + \Delta S_r$, i.e., from *stretching* and *rotation*, respectively (for a detailed calculation, see the Supplemental Material [42]).

Note that rotation is a key factor in previous auxetic materials, especially in the reentrant [13–15], rotating polygonal [16–18], and chiral models [19–21]. Thus we calculate the relative importance of area change caused by stretching versus rotation, as shown in Fig. 1(c): clearly, as the triangle deviates from the equilateral triangle at the center, the area change caused by rotation increases rapidly. When Fig. 1(b) is compared with Fig. 1(c), their similar patterns demonstrate that the negative Poisson ratio at three corners [Fig. 1(b)] corresponds nicely to the dominant area change caused by relative rotation of the bonds [Fig. 1(c)]. Thus, in a triangle lattice, the underlying mechanism of the negative Poisson ratio is due to the large area change from relative rotation of the bonds.

The above analysis comes from a regular lattice that is anisotropic, i.e., the Poisson ratio will change as the strain changes its direction (e.g., as it changes from x stretching to y stretching). However, in practice, an isotropic auxetic material that is independent of the strain direction is more preferable. Thus we design an isotropic amorphous system by distorting the lattice of equilateral triangles with a displacement $\vec{\eta}_i = (\eta \cos \varphi_i, \eta \sin \varphi_i)$ at each node, where η is the distortion magnitude and φ_i is a random distortion angle at site i [40]. At the same time, the free length of each bond changes accordingly to ensure that there is no stress in each bond. As η increases, the system becomes more and more amorphous, as shown in the Fig. 1(d) networks, and the Poisson ratio ν decreases correspondingly, as shown by the black symbols. At the same time, the local inversion symmetry also shows a similar decrease, as shown by the blue symbols [10,43,45]. Note that as we disturb the node positions, the bonds in between remain connected and the individual triangles deviate more and more from equilateral triangles, which is the main reason for a reducing ν . However, if we disconnect all the bonds and reconnect the nodes using the Delaunay triangulation protocol [46], which prevents large deviations from equilateral triangles, the Poisson ratio becomes quite stable, as shown by the red symbols. The same behavior also appears when the spring

constant is varied—e.g., inversely proportional to the bond length like a normal spring (see the Supplemental Material [42])—indicating that the geometry and the connection are more important in determining ν than the spring constant k .

To further verify our area-change mechanism, we apply a stretching strain to a specific amorphous network of triangles at $\eta = 0.325$ and the area change renormalized by the original area in each triangle is represented by the different colors in Fig. 1(e): apparently, the area change varies a lot in different triangles and we expect a large area increase to occur in triangles far from the equilateral triangle, which reduces the Poisson ratio. To check this, we calculate a geometric parameter that measures how much a triangle deviates from an equilateral triangle, the dimensionless circumcircle radius: $R = \sqrt{3}/[4 \cos(\alpha/2) \cos(\beta/2) \cos(\gamma/2)]$, where α , β , and γ are the three interior angles of the triangle [44]. The R value of each triangle is again represented by different colors in Fig. 1(f) and the values are in excellent agreement with Fig. 1(e). Therefore, a large area increase does occur in triangles far away from the equilateral triangle, which causes the decrease in the Poisson ratio and confirms our model prediction.

Clearly, triangles far away from the equilateral triangle are essential for reducing the Poisson ratio ν . Such triangles always contain either long or short bonds or both types of bonds. Therefore, at the basic single-bond level,

long or short bonds should play a crucial role in tuning ν . To understand their respective roles, we apply x stretching to the distorted network at $\eta = 0.325$ (see the y -stretching result in the Supplemental Material [42]) and obtain the forces in each bond, as plotted in Fig. 2(a). Clearly, there is a negative correlation between the tension force and the bond length, indicating that shorter bonds experience stronger stretching. We further derive the analytical expression by considering the nonaffine effects (see the Supplemental Material [42]), which are plotted as solid lines that agree well with the simulation. Because a shorter bond holds a stronger stretching force, once we remove such a bond the system area will expand, which effectively decreases the Poisson ratio ($\nu = 1 - \Delta S/(\epsilon S)$). Correspondingly, if a long bond is cut, the opposite effect occurs and ν increases. The simulation results in Fig. 2(b) prove this tuning effect, which is similar to the previous simulation in a jamming system [40], unambiguously.

The bond-cutting method is more practical than the triangle-distortion method in Fig. 1, because it can tune ν in both increasing and decreasing directions. Moreover, it works within one single network by connecting or disconnecting certain bonds, which is much simpler and practical than distorting the entire network. On the basis of this mechanism, therefore, we design and realize experimental systems. Unlike previous numerical systems that contain thousands of bonds and nodes, we design a much simpler

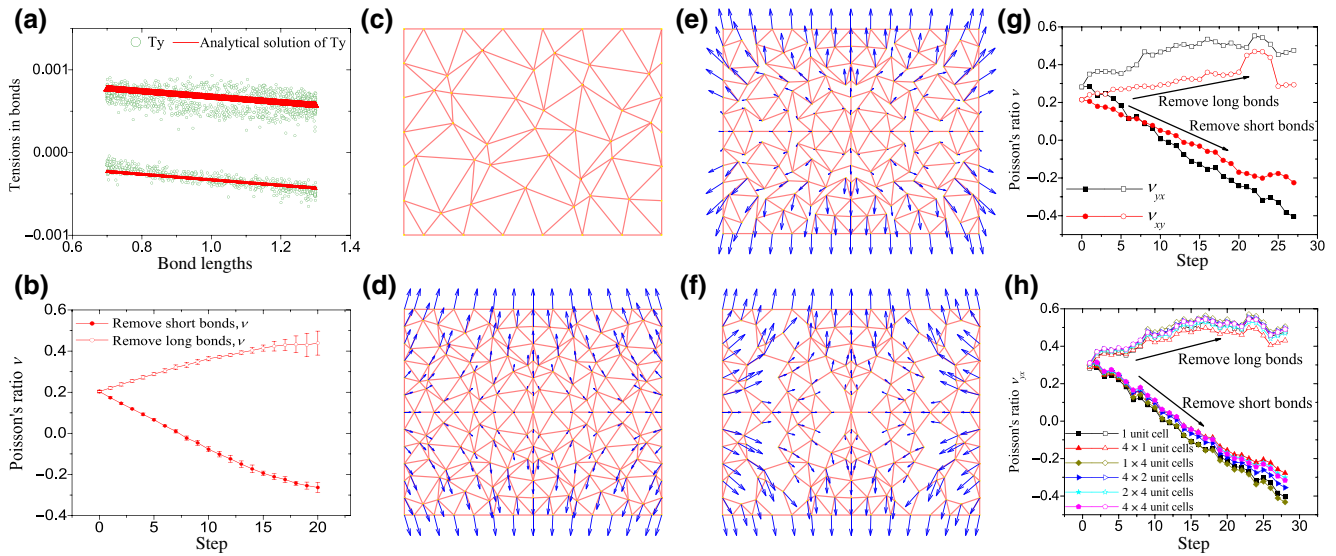


FIG. 2. (a) The tension for each bond in the distorted network shows a negative correlation with its length. T_y is the tension in each bond under a y stretching. (b) The removal of short bonds decreases ν , while the removal of long bonds increases ν . (c) A small network consisting of 56 nodes and 139 bonds distorted from an equilateral-triangular network with $\eta = 0.325$. (d) A 4×4 network constructed by mirror reflecting (a) in both the x and y directions. The blue arrows represent the displacements of each node when a stretching strain with magnitude 0.001 is imposed on the system along the y direction. The displacements are multiplied by a factor of 200 to make them visible to the eye. (e) After some short bonds are removed from the network in (b), it shows auxetic behavior. (f) After some long bonds are removed, the network shrinks more than the original structure horizontally under the external strain. (g) The removal of short or long bonds will decrease or increase ν in both the x and y directions. (h) Various large systems built from the same unit cell in (c) show the same Poisson-ratio tunability as bonds are removed.

and practical system with only 56 nodes ($N = 56$) and 139 bonds ($N_B = 139$) by distorting a regular lattice with $\eta = 0.325$, as shown in Fig. 2(c). To make the system more

isotropic, we mirror reflect this unit cell in the x and y directions to form a larger 2×2 system in Fig. 2(d), which has a positive ν around 0.25. We then gradually cut the

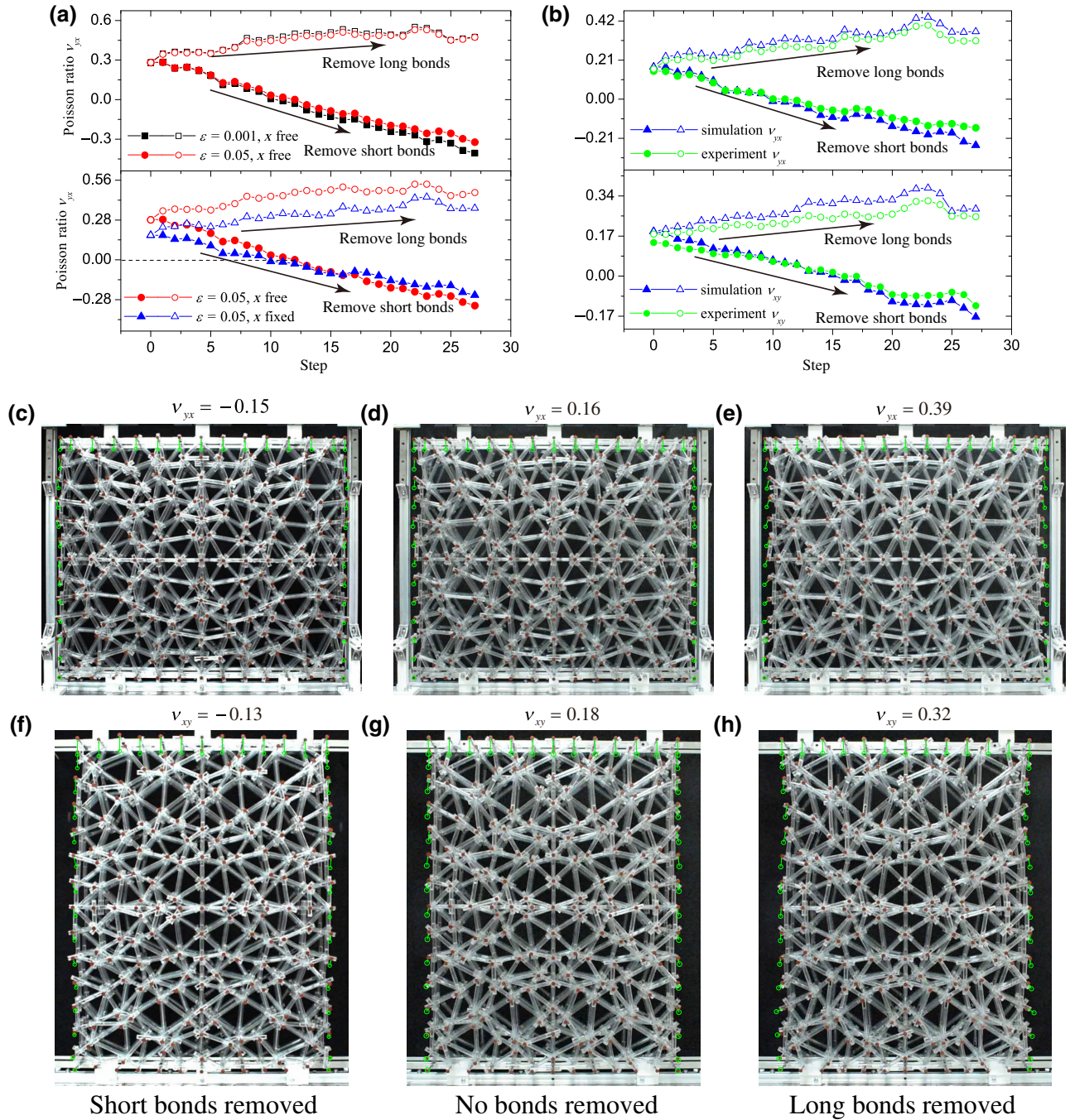


FIG. 3. (a) The top panel shows the comparison between the Poisson ratio ε_{yx} of the system under strain $\varepsilon_y = 0.001$ (black lines) and strain $\varepsilon_y = 0.05$ (red lines) during bond removal. The bottom panel shows the comparison between the Poisson ratio ε_{yx} of the system under different boundary conditions during bond removal. The red curves show that nodes of the top and bottom boundaries can move freely along the x direction. The blue curves show that the top and bottom boundary nodes are fixed along the x direction. (b) The comparison between simulation (blue lines) and experiment (green lines) under a strain of 0.05 along both the y (top panel) and the x (bottom panel) directions. (c)–(h) A comparison of the networks after bond removal. In the left column [(c),(f)], short bonds are removed. The middle column [(d),(g)] shows the original network. In the right column [(e),(h)], long bonds are removed. The green circles are the original positions of the nodes at the boundary and the green arrows indicate their displacements when the systems are stretched.

shortest 27 bonds in each unit cell to decrease ν to a negative value, as shown in Fig. 2(e). By contrast, when the longest 27 bonds are removed, ν becomes much more positive than in the original system, as shown by Fig. 2(f) versus Fig. 2(d). The exact data are shown in Fig. 2(g): note that such tuning occurs for both x stretching and y stretching, proving that the isotropic nature of our system is independent of the strain direction. Besides the 2×2 system in Fig. 2(d), we further construct systems of various sizes, such as 1×4 , 2×4 , and 4×4 , and they all exhibit excellent tuning behavior, as shown in Fig. 2(h). Thus we can construct experimental systems using this design.

III. EXPERIMENTAL REALIZATION

On the basis of the design in Fig. 2(d), we realize this mechanical metamaterial experimentally. As shown in

Figs. 3(c)–3(h), all bonds are identical springs constrained by acrylic tubes; each node is a smooth steel rod with multiple bonds attached to it. All bonds can rotate freely around each node with negligible friction; hence all of the bonds prefer to rotate rather than bend, so that the bending force is negligible and each bond exhibits a pure spring force. We can increase or decrease ν by cutting long or short bonds, as shown in Fig. 3(a). Note that similar behavior appears under different experimental conditions such as the strain magnitude (upper panel) and the boundary conditions (lower panel), demonstrating the robustness of our system. The experimental results agree well with simulations under both x stretching and y stretching, as shown in Fig. 3(b).

The actual system responses are shown in Figs. 3(c)–3(h): the left, middle, and right columns respond to short-bond removal, the original system, and long-bond removal,

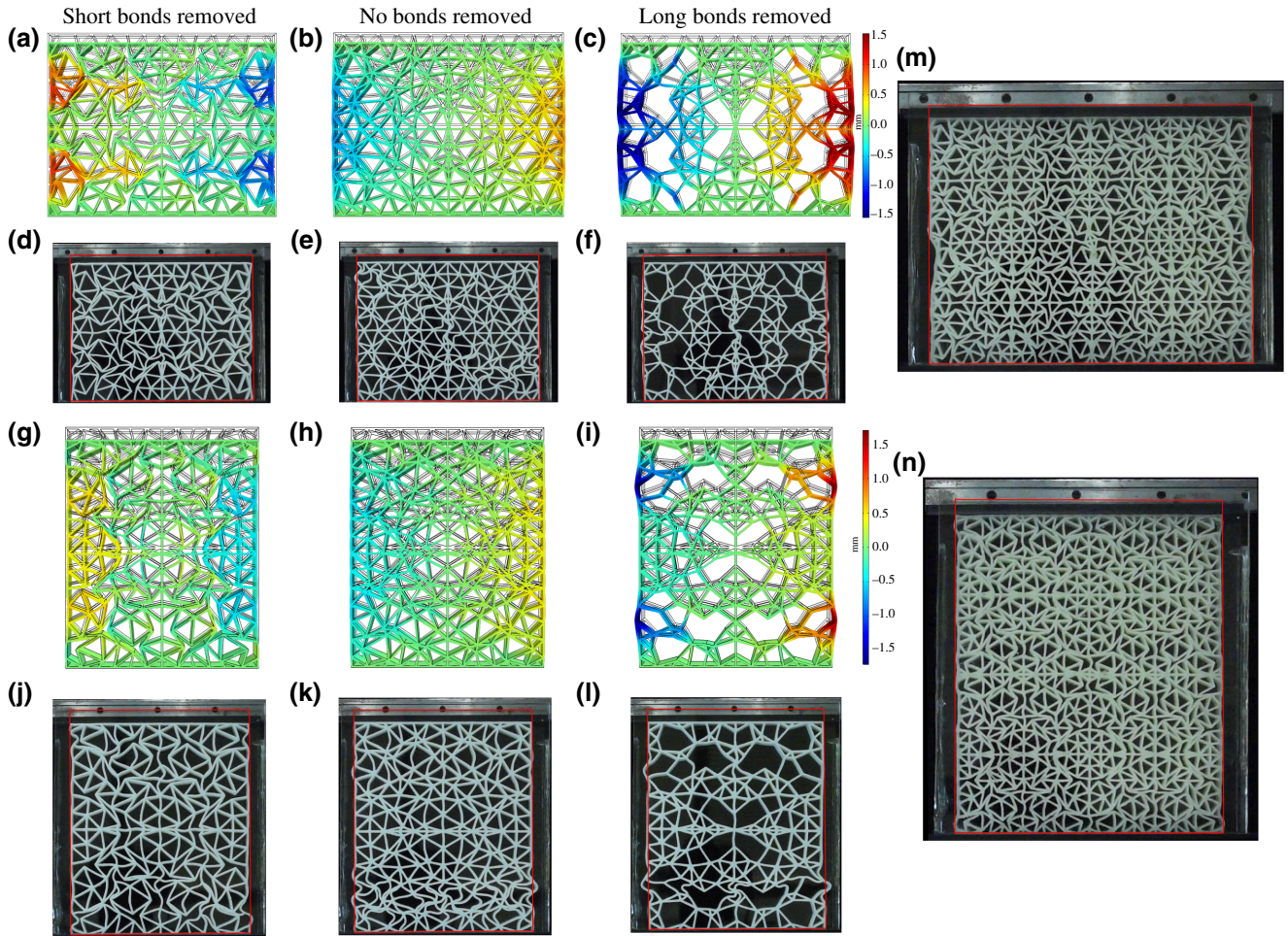


FIG. 4. The 3D printing systems with a tunable Poisson ratio. The colorful rows are the simulation results and the images below are the corresponding experiments. (a),(d),(g),(j) The removal of short bonds causes a negative ν . (b),(e),(h),(k) The original structure. (c),(f),(i),(l) The removal of long bonds increases ν . The top two rows and the bottom two rows are rotated by 90° for both x compression and y compression. (m),(n) The deformations of a large system built from the unit cell. The red lines around the experimental systems indicate the position of the boundary before the compressing pressure is applied.

respectively. The green circles are the original boundary node positions and the arrows show their displacements under vertical stretching. We rotate the system by 90° in the top and bottom panels to apply y and x stretching, respectively. Compared with the original positive- ν system in the middle, the system in the left column expands horizontally, which indicates a negative ν ; while the system on the right shrinks more than the middle, which confirms a more positive ν . The forms of behavior after the removal of short and long bonds are more clearly shown in Videos 1 and 2 of the Supplemental Material [42]; and the effect of each bond removal is demonstrated in Videos 3 and 4 of the Supplemental Material [42].

Even beyond the spring network, we further construct more general elastic networks with 3D printing, the bonds in which exhibit bending and twisting under strain, which is beyond the present model. Nevertheless, the simulations and experiments shown in Figs. 4(a)–4(l) demonstrate a similar tunability in ν by cutting short and long bonds, despite the disturbances from bending and twisting (see the experiment under x compression and y compression in Videos 5 and 6 of the Supplemental Material [42]). This indicates the robustness of our approach. However, we also point out that the bending and twisting reduces the tunability range, which can be studied in the future. Moreover, we use Fig. 4(a) as the unit cell to form a much larger system with a negative ν , the deformations of which under x compression and y compression are shown in Figs. 4(m) and 4(n) (see Videos 7 and 8 in the Supplemental Material [42]). Similarly, this large system is auxetic for both directions, demonstrating the potential of our design to achieve large isotropic systems.

IV. CONCLUSIONS

To conclude, starting from the regular triangular lattice, we find that ν has a close relationship with the geometry of the individual triangle, i.e., triangles deviating far away from the equilateral triangle will have a large area change under strain, thus resulting in a decreasing or even negative Poisson ratio. In addition, we prove that the nonaffinity of the network leads to a negative correlation between the bond length and their tension and thus the removal of short or long bonds can decrease or increase ν , respectively. All such tunability can be experimentally realized in both the spring network and the 3D-printed elastic network. Triangles far away from an equilateral triangle may contain very long bonds, which violates the normal situation in which significant interactions usually occur among nearby nodes or particles. The removal of short bonds further magnifies this anomaly. We suspect that a negative Poisson ratio or auxetic behavior originates from this anomaly. To summarize, with triangular analysis, our study provides a practical design principle for mechanical metamaterials with a tunable Poisson ratio.

ACKNOWLEDGMENTS

We acknowledge financial support from NSFC, under Grant No. 12074325, from Hong Kong RGC, under Grants No. GRF-14306518, No. CRF-C6016-20G, and No. CRF-C1018-17G, from the Chinese University of Hong Kong, under Direct Grant No. 4053354, from the Guangdong Basic and Applied Basic Research Foundation, under Grant No. 2021A1515110524, and from the China Postdoctoral Science Foundation, under Grants No. 2021M702283 and No. 2022T150438.

Z.J. and C.F. contributed equally to this work.

- [1] G. N. Greaves, A. Greer, R. S. Lakes, and T. Rouxel, Poisson's ratio and modern materials, *Nat. Mater.* **10**, 823 (2011).
- [2] S. Poisson, Note sur l'extension des fils et des plaques élastiques, *Ann. Chim. Phys.* **36**, 384 (1827).
- [3] H. M. Kolken and A. Zadpoor, Auxetic mechanical metamaterials, *RSC Adv.* **7**, 5111 (2017).
- [4] X. Ren, R. Das, P. Tran, T. D. Ngo, and Y. M. Xie, Auxetic metamaterials and structures: A review, *Smart Mater. Struct.* **27**, 023001 (2018).
- [5] J.-P. Poirier, *Introduction to the Physics of the Earth's Interior* (Cambridge University Press, Cambridge, 2000).
- [6] A. E. H. Love, *A Treatise on the Mathematical Theory of Elasticity* (Cambridge University Press, Cambridge, 2013).
- [7] A. Zaccone and E. M. Terentjev, Short-range correlations control the g/k and Poisson ratios of amorphous solids and metallic glasses, *J. Appl. Phys.* **115**, 033510 (2014).
- [8] M. Schlegel, J. Brujic, E. Terentjev, and A. Zaccone, Local structure controls the nonaffine shear and bulk moduli of disordered solids, *Sci. Rep.* **6**, 1 (2016).
- [9] A. Zaccone and E. Scossa-Romano, Approximate analytical description of the nonaffine response of amorphous solids, *Phys. Rev. B* **83**, 184205 (2011).
- [10] B. Cui, G. Ruocco, and A. Zaccone, Theory of elastic constants of athermal amorphous solids with internal stresses, *Granul. Matter* **21**, 69 (2019).
- [11] K. E. Evans, M. Nkansah, I. Hutchinson, and S. Rogers, Molecular network design, *Nature* **353**, 124 (1991).
- [12] R. Lakes, Foam structures with a negative Poisson's ratio, *Science* **235**, 1038 (1987).
- [13] K. E. Evans, M. Nkansah, and I. Hutchinson, Auxetic foams: Modelling negative Poisson's ratios, *Acta Metall. et Mater.* **42**, 1289 (1994).
- [14] I. Masters and K. Evans, Models for the elastic deformation of honeycombs, *Compos. Struct.* **35**, 403 (1996).
- [15] L. Yang, O. Harrysson, H. West, and D. Cormier, Mechanical properties of 3D re-entrant honeycomb auxetic structures realized via additive manufacturing, *Int. J. Solids Struct.* **69**, 475 (2015).
- [16] J. N. Grima and K. E. Evans, Auxetic behavior from rotating squares, *J. Mater. Sci. Lett.* **19**, 1563 (2000).
- [17] A. Alderson and K. Evans, Rotation and dilation deformation mechanisms for auxetic behaviour in the α -cristobalite tetrahedral framework structure, *Phys. Chem. Miner.* **28**, 711 (2001).

- [18] A. Rafsanjani and D. Pasini, Bistable auxetic mechanical metamaterials inspired by ancient geometric motifs, *Extreme Mech. Lett.* **9**, 291 (2016).
- [19] R. Lakes, Deformation mechanisms in negative Poisson's ratio materials: Structural aspects, *J. Mater. Sci.* **26**, 2287 (1991).
- [20] C. S. Ha, M. E. Plesha, and R. S. Lakes, Chiral three-dimensional lattices with tunable Poisson's ratio, *Smart Mater. Struct.* **25**, 054005 (2016).
- [21] D. Prall and R. Lakes, Properties of a chiral honeycomb with a Poisson's ratio of -1 , *Int. J. Mech. Sci.* **39**, 305 (1997).
- [22] L. J. Hall, V. R. Coluci, D. S. Galvão, M. E. Kozlov, M. Zhang, S. O. Dantas, and R. H. Baughman, Sign change of Poisson's ratio for carbon nanotube sheets, *Science* **320**, 504 (2008).
- [23] F. Scarpa, S. Adhikari, and A. S. Phani, Effective elastic mechanical properties of single layer graphene sheets, *Nanotechnology* **20**, 065709 (2009).
- [24] J. N. Grima, S. Winczewski, L. Mizzi, M. C. Grech, R. Cauchi, R. Gatt, D. Attard, K. W. Wojciechowski, and J. Rybicki, Tailoring graphene to achieve negative Poisson's ratio properties, *Adv. Mater.* **27**, 1455 (2015).
- [25] J. N. Grima and R. Gatt, Perforated sheets exhibiting negative Poisson's ratios, *Adv. Eng. Mater.* **12**, 460 (2010).
- [26] L. Mizzi, K. M. Azzopardi, D. Attard, J. N. Grima, and R. Gatt, Auxetic metamaterials exhibiting giant negative Poisson's ratios, *Phys. Status Solidi (RRL)—Rapid Res. Lett.* **9**, 425 (2015).
- [27] A. Yeganeh-Haeri, D. J. Weidner, and J. B. Parise, Elasticity of α -cristobalite: A silicon dioxide with a negative Poisson's ratio, *Science* **257**, 650 (1992).
- [28] N. R. Keskar and J. R. Chelikowsky, Negative Poisson ratios in crystalline SiO_2 from first-principles calculations, *Nature* **358**, 222 (1992).
- [29] R. H. Baughman, J. M. Shacklette, A. A. Zakhidov, and S. Stafström, Negative Poisson's ratios as a common feature of cubic metals, *Nature* **392**, 362 (1998).
- [30] H. Qin, Y. Sun, J. Z. Liu, M. Li, and Y. Liu, Negative Poisson's ratio in rippled graphene, *Nanoscale* **9**, 4135 (2017).
- [31] R. H. Baughman, Auxetic materials: Avoiding the shrink, *Nature* **425**, 667 (2003).
- [32] S. Pagliara, K. Franze, C. R. McClain, G. W. Wylde, C. L. Fisher, R. J. Franklin, A. J. Kabla, U. F. Keyser, and K. J. Chalut, Auxetic nuclei in embryonic stem cells exiting pluripotency, *Nat. Mater.* **13**, 638 (2014).
- [33] B. Xu, F. Arias, S. T. Brittain, X.-M. Zhao, B. Grzybowski, S. Torquato, and G. M. Whitesides, Making negative Poisson's ratio microstructures by soft lithography, *Adv. Mater.* **11**, 1186 (1999).
- [34] K. E. Evans and A. Alderson, Auxetic materials: Functional materials and structures from lateral thinking! *Adv. Mater.* **12**, 617 (2000).
- [35] J. N. Grima, R. Jackson, A. Alderson, and K. E. Evans, Do zeolites have negative Poisson's ratios? *Adv. Mater.* **12**, 1912 (2000).
- [36] Y. Tang and J. Yin, Design of cut unit geometry in hierarchical kirigami-based auxetic metamaterials for high stretchability and compressibility, *Extreme Mech. Lett.* **12**, 77 (2017).
- [37] C. P. Goodrich, A. J. Liu, and S. R. Nagel, The Principle of Independent Bond-Level Response: Tuning by Pruning to Exploit Disorder for Global Behavior, *Phys. Rev. Lett.* **114**, 225501 (2015).
- [38] D. R. Reid, N. Pashine, J. M. Wozniak, H. M. Jaeger, A. J. Liu, S. R. Nagel, and J. J. de Pablo, Auxetic metamaterials from disordered networks, *Proc. Nat. Acad. Sci.* **115**, E1384 (2018).
- [39] V. F. Hagh and M. Thorpe, Disordered auxetic networks with no reentrant polygons, *Phys. Rev. B* **98**, 100101 (2018).
- [40] J. Liu, Y. Nie, H. Tong, and N. Xu, Realizing negative Poisson's ratio in spring networks with close-packed lattice geometries, *Phys. Rev. Mater.* **3**, 055607 (2019).
- [41] X. Shen, C. Fang, Z. Jin, H. Tong, S. Tang, H. Shen, N. Xu, J. H. Y. Lo, X. Xu, and L. Xu, Achieving adjustable elasticity with non-affine to affine transition, *Nat. Mater.* **20**, 1635 (2021).
- [42] See the Supplemental Material at <http://link.aps.org/supplemental/10.1103/PhysRevApplied.18.054052>, which includes Ref. [47], for the detailed derivation of the Poisson ratio.
- [43] R. Milkus and A. Zaccone, Local inversion-symmetry breaking controls the boson peak in glasses and crystals, *Phys. Rev. B* **93**, 094204 (2016).
- [44] B. Yu, M. Lin, and W. Tao, Automatic generation of unstructured grids with Delaunay triangulation and its application, *Heat Mass Transfer* **35**, 361 (1999).
- [45] C. L. Kelchner, S. J. Plimpton, and J. C. Hamilton, Dislocation nucleation and defect structure during surface indentation, *Phys. Rev. B* **58**, 11085 (1998).
- [46] B. Delaunay, *et al.*, Sur la sphere vide, *Izv. Akad. Nauk SSSR, Otdelenie Matematicheskii i Estestvennyka Nauk* **7**, 1 (1934).
- [47] T. Lubensky, C. Kane, X. Mao, A. Souslov, and K. Sun, Phonons and elasticity in critically coordinated lattices, *Rep. Prog. Phys.* **78**, 073901 (2015).